ACCOUNTS of chemical research

Article

pubs.acs.org/accounts

Ultrafast Exciton Dynamics and Light-Driven H_2 Evolution in Colloidal Semiconductor Nanorods and Pt-Tipped Nanorods

Published as part of the Accounts of Chemical Research special issue "Ultrafast Excited-State Processes in Inorganic Systems".

Kaifeng Wu, Haiming Zhu, and Tianquan Lian*

Department of Chemistry, Emory University, Atlanta, Georgia 30322, United States

CONSPECTUS: Colloidal quantum confined one-dimensional (1D) semiconductor nanorods (NRs) and related semiconductor−metal heterostructures are promising new materials for efficient solar-to-fuel conversion because of their unique physical and chemical properties. NRs can simultaneously exhibit quantum confinement effects in the radial direction and bulk like carrier transport in the axial direction. The former implies that concepts well-established in zero-dimensional quantum dots, such as size-tunable energetics and wave function engineering through band alignment in heterostructures, can also be applied to NRs; while the latter endows NRs with fast carrier transport to achieve long distance charge separation. Selective growth of catalytic metallic nanoparticles, such as Pt, at the tips of NRs provides convenient routes to multicomponent heterostructures with photocatalytic capabilities and controllable charge separation distances. The design and optimization of such materials for efficient solar-to-fuel conversion require the understanding of exciton and charge carrier dynamics.

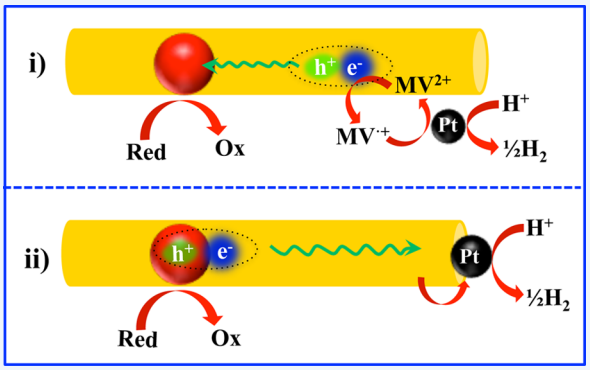

In this Account, we summarize our recent studies of ultrafast charge separation and recombination kinetics and their effects on steady-state photocatalytic efficiencies of colloidal CdS and CdSe/CdS NRs and related NR-Pt heterostructures. After a brief introduction of their electronic structure, we discuss exciton dynamics of CdS NRs. By transient absorption and time-resolved photoluminescence decay, it is shown that although the conduction band electrons are long-lived, photogenerated holes in CdS NRs are trapped on an ultrafast time scale (~0.7 ps), which forms localized excitons due to strong Coulomb interaction in 1D NRs. In quasi-type II CdSe/CdS dot-in-rod NRs, a large valence band offset drives the ultrafast localization of holes to the CdSe core, and the competition between this process and ultrafast hole trapping on a CdS rod leads to three types of exciton species with distinct spatial distributions. The effect of the exciton dynamics on photoreduction reactions is illustrated using methyl viologen (MV^{2+}) as a model electron acceptor. The steady-state MV^{2+} photoreduction quantum yield of CdSe/CdS dot-in-rod NRs approaches unity under rod excitation, much larger than CdSe QDs and CdSe/CdS core/shell QDs. Detailed time-resolved studies show that in quasi-type II CdSe/CdS NRs and type II ZnSe/CdS NRs strong quantum confinement in the radial direction facilitates fast electron transfer and hole removal, whereas the fast carrier mobility along the axial direction enables long distance charge separation and slow charge recombination, which is essential for efficient MV^{2+} photoreduction. The NR/MV^{2+} relay system can be coupled to Pt nanoparticles in solution for light-driven H_2 generation. Alternatively, Pt-tipped CdS and CdSe/CdS NRs provide fully integrated all inorganic systems for light-driven H_2 generation. In CdS-Pt and CdSe/CdS-Pt hetero-NRs, ultrafast hole trapping on the CdS rod surface or in CdSe core enables efficient electron transfer from NRs to Pt tips by suppressing hole and energy transfer. It is shown that the quantum yields of photodriven H_2 generation using these heterostructures correlate well with measured hole transfer rates from NRs to sacrificial donors, revealing that hole removal is the key efficiency-limiting step. These findings provide important insights for designing more efficient quantum confined NR and NR-Pt based systems for solar-to-fuel conversion.

1. INTRODUCTION

Recent advances in nanocrystal size and shape control have led to the synthesis of colloidal quantum-confined one-dimensional (1D) semiconductor nanostructures, such as nanorods (NRs) and tetrapods.[1−4] Unlike zero-dimensional (0D) quantum dots (QDs),[5] in which the exciton is quantum confined in all three dimensions, exciton motions in 1D NRs (with diameters of a few nanometers and lengths of 10−100 nm) are quantum confined in the radial direction but are bulk-like along the axial direction.[6−8] Thus, NRs can simultaneously possess the properties of quantum confined nanocrystals and bulk crystals.

Received: October 31, 2014
Published: February 16, 2015

DOI: 10.1021/ar500398g
Acc. Chem. Res. 2015, 48, 851−859

It has been well demonstrated that in core/shell QD heterostructures, the spatial distribution of conduction band (CB) electrons and valence band (VB) holes in excitonic states can be tuned by the sizes and compositions of the constituent materials to control their photophysical properties, including the lifetimes of single and multiple excitons in QDs and the rates of charge separation and recombination in QD−acceptor complexes.[9] This wave function engineering concept can also be applied to NR-based heterostructures,[10] such as dot-in-rod NRs,[11−13] tetrapods,[11,12] and nanobarbells.[14,15] Furthermore, because the tips of NRs are often associated with high-energy crystal faces,[16] selective growth of metal nanoparticles (such as platinum and gold[16,17]) at the tip can be readily achieved. Thus, in principle, these integrated triadic semiconductor/metal NR heterostructures, consisting of well positioned light absorbing, charge separating, and catalytic components, can be ideal materials for solar-to-fuel conversion.[18−21]

The overall light-driven catalytic conversion reaction involves many forward and backward elementary steps. Using triadic CdSe/CdS−Pt NRs as a model system, some of these steps are depicted in Scheme 1.[22] In an ideal quasi-type II hetero-NR, VB holes in CdS are driven to the CdSe core (with a time constant of τ_{HL}) by valence band offset,[23,24] while CB electrons can be dissociated from holes and transported to the Pt domain (τ_{ET}). This long distance spatial separation of electrons and holes in the axial direction over three domains prolongs the lifetime of the charge-separated states (CS). The strong quantum confinement in the radial direction also facilitates fast hole removal by electron donor (τ_{HT}), which enables the accumulation of electrons in the Pt tip to carry out reduction of two protons to form H_2 (τ_{CAT}). These forward charge separation steps compete with backward recombination processes, including the intrinsic electron−hole recombination within the NR (τ_{IN}) and the loss of electrons in the Pt by recombination with the holes in the CdSe (τ_{CR}) and with the oxidized donor (τ_L). Furthermore, due to large surface to volume ratio, photogenerated carriers are susceptible to trapping along the rod,[18,25] which can localize excitons at the trap sites through the large electron−hole binding energy in NRs.[8,24,25] Thus, rational improvement of the photocatalytic efficiencies in such triadic nanoheterostructures requires a detailed understanding of the rates of these competing processes and their dependences on the constituent materials, dimensions, and surface properties.

In this Account, we summarize our recent studies of exciton transport, charge separation, and recombination dynamics in CdSe/CdS and CdSe/CdS/Pt colloidal NRs and related heterostructures and their relationship to light-driven redox mediator generation and H_2 evolution. After a brief description of NR electronic structure in section 2, the dynamics of excitons in CdS and CdSe/CdS NRs are discussed in sections 3 and 4, respectively. The implication of the exciton dynamics on steady-state photoreduction of MV^{2+} is discussed in section 5. The mechanisms of charge separation and recombination in CdS/Pt and CdSe/CdS/Pt NRs are described in section 6, which is followed by a discussion of efficiency limiting factors in solar-driven H_2 generation in section 7. Finally, we conclude and point out some future research directions in this field.

Scheme 1. Photogeneration of H_2 in CdSe/CdS−Pt Triadic NRs[a]

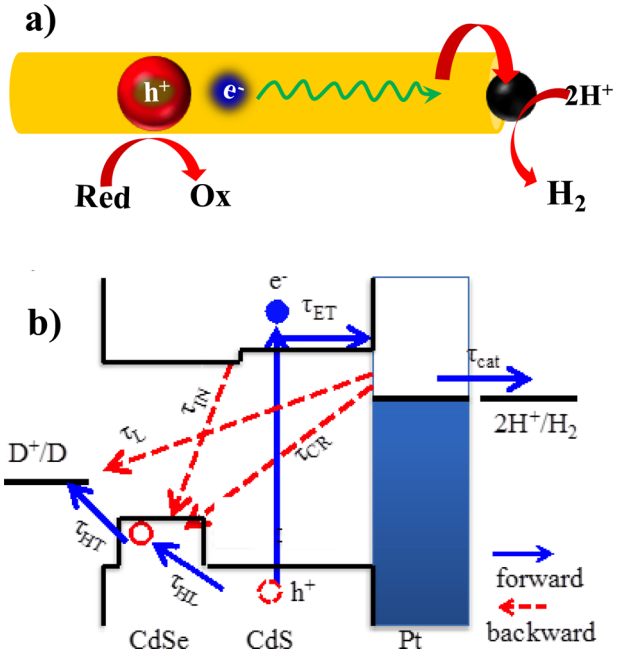

[a](a) Schematic illustration of a triadic NR: a CdSe core embedded in a CdS NR with a Pt nanoparticle at one tip. Upon photoexcitation, electrons are transferred to Pt tip for the catalytic reduction of $2H^+$ to H_2, while holes are transferred to the CdSe core and then removed by external electron donors. (b) Schematic diagram showing relative energy levels in CdSe, CdS, and Pt and charge separation (forward) and recombination (backward) processes relevant to photocatalytic H_2 generation. See the main text for details. Adapted with permission from ref 22. Copyright 2014 American Chemical Society.

2. ELECTRONIC STRUCTURE OF NANORODS

The static absorption spectra of three CdS NRs with similar diameters but different lengths are displayed in Figure 1a.[26] It illustrates that when the length of NR is much larger than exciton Bohr diameter (~5.5 nm in bulk CdS[27,28]), the excitonic transition energies are determined by the rod diameter. In NRs with cylindrical symmetry, quantum confine-

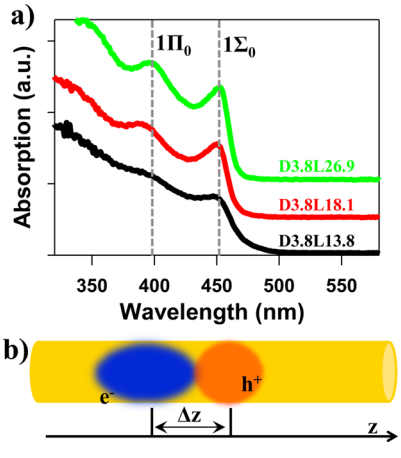

Figure 1. Electronic structure and optical property of NRs. (a) Static absorption spectra of three CdS NRs with similar diameters (3.8 nm) and different lengths (L). (b) Illustration of fast electron and hole motions in the quantum confined radial direction and the effective 1D Coulomb interaction, $V_{e-h}(\Delta z)$, that gives rise to 1D bound exciton states in NRs. The center of mass of this bound exciton is free to move along the axial direction.

DOI: 10.1021/ar500398g
Acc. Chem. Res. 2015, 48, 851−859

ment in the radial direction leads to discrete electron and hole levels labeled as 1σ, 1π, etc.[8,29] Because the carrier motion in the radial direction is much faster than that in the axial direction, electron−hole interaction (V_{e-h}) can be described by an effective 1D Coulomb potential that depends on their separation along the long axis of the NR (Figure 1b). This 1D potential between the 1σ (π) electron and hole forms a manifold of bound $1\Sigma(\Pi)$ exciton states with the oscillator strength largely concentrated on the lowest energy exciton state, $1\Sigma_0(1\Pi_0)$.[8,29] Following this model, the peaks at ~390 and 450 nm can be attributed to the lowest energy $1\Pi_0$ and $1\Sigma_0$ transitions, respectively, as shown in Figure 1a.[8,18] It is also important to note that as a general property of 1D materials, the exciton binding energy in NRs (on the order of hundreds of millielectronvolts[8]) is much larger than that in QDs, due to reduced dielectric screening.[30−32]

3. EXCITON DYNAMICS IN CdS NANORODS: EFFECT OF HOLE TRAPPING

Realistic electronic structure of colloidal NRs deviates from the picture in Figure 1b due to the presence of trap states within the band gap. As shown in Figure 2a, the photoluminescence

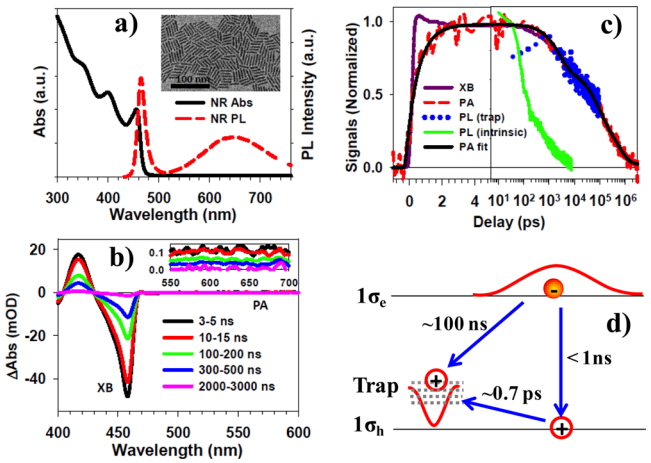

Figure 2. TA spectra and kinetics of CdS NRs. (a) Static absorption (black solid line) and photoluminescence (PL, red dashed line) spectra of CdS NRs (TEM in the inset). (b) TA spectra of CdS NRs at indicated delays after 400 nm excitation, showing XB and PA (zoom-in inset) features. (c) TA kinetics of XB (purple solid line) and PA (red dashed line), time-resolved PL decay kinetics of trap state (blue dots) and band edge (green solid line), and a multiexponential fit of PA kinetics (black solid line). (d) A scheme showing electron and hole processes in CdS NRs. Adapted with permission from ref 18. Copyright 2012 American Chemical Society.

(PL) spectrum of CdS NRs shows two distinct emission bands, with a narrow band-edge emission at 463 nm and a broad trap-state emission centered at 650 nm.[33] The effect of traps states on exciton dynamics can be best probed by combining transient absorption spectroscopy and time-resolved photoluminescence. The transient absorption (TA) spectra of CdS NRs after 400 nm excitation (Figure 2b) show a bleach of the $1\Sigma_0$ exciton band (XB) at ~456 nm and a much weaker and broader photoinduced absorption (PA) band at >500 nm. Removal of CB electrons by electron acceptors leads to the complete recovery of XB signal and does not change the PA signal, suggesting that the XB is due to state filling of the 1σ electron level and the PA signal can be assigned to holes.[18] Furthermore, the decay kinetics of both PA and XB features agree with the trap state emission decay (Figure 2c), suggesting that PA can be assigned to trapped holes in CdS NRs. Thus, as summarized in Figure 2d, ultrafast trapping of VB holes (with a time constant of 0.7 ps) leads to long-lived (~100 ns) trapped excitons (i.e., CB electrons bound to trapped holes). Despite ultrafast hole trapping, noticeable band edge emission can still be observed, which can be attributed to its much larger radiative decay rate than trapped excitons as well as a small of portion of NRs without ultrafast hole trapping processes.[18] The consequence of ultrafast hole trapping on exciton transport and dissociation dynamics in heterostructures will be discussed later.

4. CdSe/CdS DOT-IN-ROD NANORODS: COMPETITION BETWEEN BAND ALIGNMENT AND TRAPPING DRIVEN EXCITON DYNAMICS

In CdSe/CdS dot-in-rod NRs, the VB offset between CdSe and CdS (>0.45 eV) provides a driving force for localizing the hole to the CdSe core,[11,12] whereas the electron wave functions can delocalize into CdS due to small CB offset (<0.3 eV) and stronger quantum confinement in the CdSe core.[34,35] Although promising photocatalytic performances of CdSe/CdS NRs have been reported,[21,36,37] the effects of this quasi-type II band alignment on exciton dynamics and the extent of CB electron delocalization were not well understood.[24]

Dot-in-rod NRs grown by seeded growth methods often show a bulb region (rod material surrounding the seed) with diameters larger than the rod (Figure 3a). The absorption spectrum of CdSe/CdS NRs with an average length ~17 nm and diameter of ~3.5 nm (Figure 3b) can be fit by the sum of

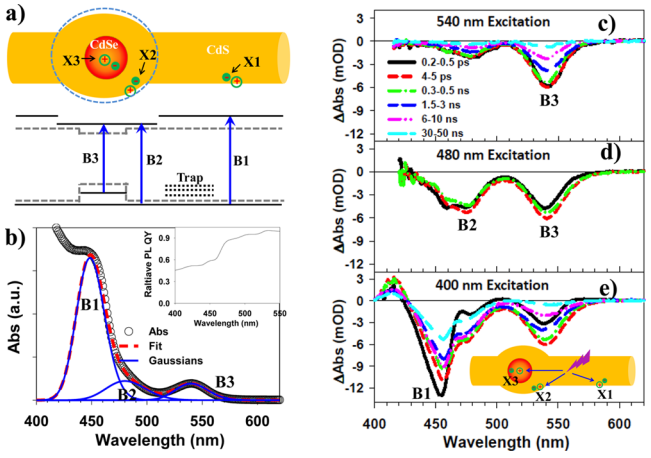

Figure 3. Hole-localization driven formation of three spatially separated excitons in CdSe/CdS dot-in-rod NRs. (a) Scheme and energy level diagram of a CdSe/CdS NR with a bulb surrounding the core: bulk band edge positions of CdS and CdSe (gray dotted lines), lowest CB electron, and VB hole energy levels in CdSe core, CdS bulb, and CdS rod (black solid lines) and sub-band gap hole trapping states on CdS rod (black dotted lines). Also shown are the lowest energy transitions in CdS rod (B1), CdS bulb (B2), and CdSe core (B3) and excitons localized in these domains (X1, X2, and X3, respectively). (b) Static absorption spectrum of CdSe/CdS NRs (black circles) and its fit (red dashed line) to three Gaussian bands (blue solid lines). (c−e) TA spectra of CdSe/CdS NRs at indicated delays after (c) 540, (d) 480, and (e) 400 nm excitations. The inset is a scheme showing that the 400 nm excitation generated electron−hole pair is branched into three types of long-lived excitons, X1, X2, and X3. Adapted with permission from ref 24. Copyright 2013 American Chemical Society.

DOI: 10.1021/ar500398g
Acc. Chem. Res. 2015, 48, 851−859

three Gaussian bands with centers at 449, 480, and 539 nm, corresponding to lowest excitonic states in the CdS NR, CdS bulb surrounding the core, and CdSe core, respectively. They are labeled as B1, B2, and B3 transitions in the energy level diagram in Figure 3a. We note that the $2S_{3/2}(h)-1S(e)$ transition in the CdSe core may also appear at ~480 nm, but the CdS bulb transition should dominate because of its much larger absorption cross section. The excitation wavelength-dependent relative photoluminescence (PL) quantum yields (QYs) show decreasing QYs at shorter wavelengths (Figure 3a, inset). Specifically, the relative QYs at 400, 480, and 540 nm excitations are ~0.46, ~0.87, and 1, respectively. Assuming that all NRs contain a CdSe core, this result indicates that some of the excitons generated at the CdS rod and bulb region do not localize to the CdSe core and remain trapped on these regions. The excitons trapped on CdS rod and CdS bulb and confined in CdSe core are labeled as X1, X2, and X3, respectively (Figure 3a).

Transient absorption measurements were carried out to reveal the dependence of exciton localization dynamics on the excitation wavelength. Resonant excitation of the CdSe core at B3 transition (540 nm) generates X3 excitons with holes in the CdSe (Figure 3a). TA spectra (Figure 3c) show strong bleach of the CdSe exciton (B3) and small bleach of the CdS bulb exciton (B2). Since these bleach features are caused by state-filling of the electron levels,[18,37−40] the presence of both B3 and B2 bleach suggests that in the X3 exciton state, the CB electrons are delocalized among the CdSe core and the CdS bulb, consistent with a quasi-type II band alignment.[41,42] TA spectra at 480 nm excitation (Figure 3d) show both B2 and B3 bleaches, although the amplitude of B2 relative to B3 is larger than that for the 540 nm excitation, suggesting that some of the CB electrons lead to B2 but not B3 bleach. This is attributed to trapped excitons with holes localized at the bulb surface (X2, Figure 3a) and is consistent with the relative PL QY of 0.87 at 480 nm. The 400 nm light (Figure 3e) mostly excites the CdS NR region due to its much larger volume (and larger extinction coefficient) than the CdSe core and CdS bulb;[34] 53% of the CdS NR bleach (B1) decays to form B2 and B3 bleach with a time constant of ~0.42 ps, which can be assigned to the transfer of excitons from CdS NR to CdS bulb (X2) and CdSe core (X3). The remaining B1 bleach is long-lived, due to hole trapping induced exciton localization on the CdS rod (X1). In our NRs, the percentages of X1, X2, and X3 are 47%, 7%, and 46%, respectively.[24] These branching ratios are determined by the competition between hole trapping on CdS rod and CdS bulb and hole localization to CdSe core, which likely depends sensitively on the microscopic electronic and morphological heterogeneity of the materials. The presence of multiple types of excitonic species is also observed in ZnSe/CdS NRs.[43] The distinct spatial locations of these excitons have important effects on the applications of these NRs as the light harvesting materials for solar energy conversion.

5. CdSe/CdS AND ZnSe/CdS NANORODS FOR PHOTOCATALYSIS

The capability of NRs and NR heterostructures to trap or localize holes motivated us to apply them for photocatalysis. The model reaction we examined is the photoreduction of methyl viologen (MV^{2+}), a well-known fast electron acceptor[38,40] and redox mediator for H_2 evolution.[37,44,45] Figure 4a compares the initial $MV^{+\bullet}$ radical generation quantum yields (QYs) of different nanostructures, including $Ru(bipy)_3^{2+}$ (bipy = 2,2′-bipyridine) molecules, CdSe core only QDs, CdSe/CdS core/shell QDs, CdS NRs, and CdSe/CdS NRs. All nanocrystals were transferred to the aqueous phase by replacing their native ligands with mercaptopropionic acid (MPA), which also acts as a sacrificial electron donor to remove holes in nanocrystals. Under our experimental conditions, the QYs show the following trend: CdSe/CdS NRs (~98%) > CdS NRs (~65%) > CdSe/CdS core/shell QDs (~31%) > $Ru(bipy)_3^{2+}$ (~20%) > CdSe QD (~11%).[37] Especially impressive is the near unity QY of CdSe/CdS NRs. Addition of Pt nanoparticles to these systems leads to the formation of H_2 with relative QYs following the trend of MV^{2+} photoreduction.[37]

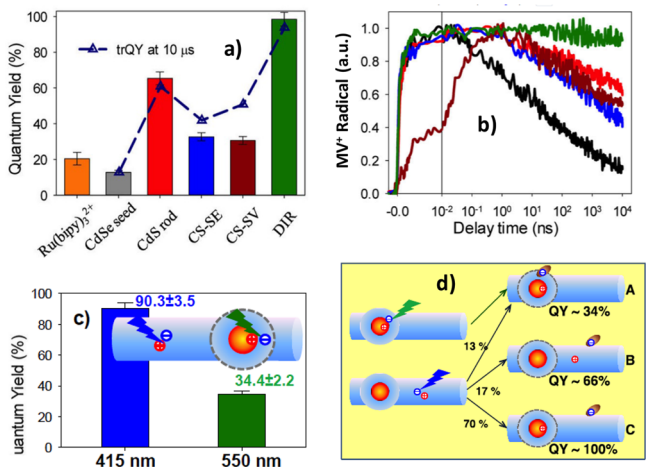

Figure 4. Efficient photoreduction of methyl viologen (MV^{2+}) using dot-in-rod (DIR) nanorods. (a) $MV^{+\bullet}$ radical photogeneration QYs using different nanomaterials: $Ru(bipy)_3^{2+}$, CdSe QD seed, CdS NR, CdSe/CdS DIR, CdSe/CdS core/shell QDs of similar lowest exciton energy (CS-SE), and CdSe/CdS core/shell QDs of similar volume (CS-SV) as the DIR. Also plotted are the transient quantum yields (open triangles) at 10 us obtained from TA measurements. (b) Comparison of the formation and decay kinetics of $MV^{+\bullet}$ radicals generated by 400 nm excitation of aqueous solutions containing different NCs (same color scheme as panel a). (c) $MV^{+\bullet}$ radical generation QYs of ZnSe/CdS DIRs under 415 and 550 nm excitations. (d) Schematic depiction of charge-separated states A, B, and C generated in ZnSe/CdS DIR−MV^{2+} complexes after excitation at the bulb and rod regions. Panels a and b are adapted with permission from ref 37. Copyright 2012 American Chemical Society. Panels c and d are adapted with permission from ref 43. Copyright 2014 Royal Society of Chemistry.

TA kinetics shows that in all systems, the initial formation of $MV^{+\bullet}$ radicals is fast and 100% efficient, but the lifetimes of $MV^{+\bullet}$ radicals differ (Figure 4b). The trends of both radical lifetimes (Figure 4b) and transient QYs at 10 μs (Figure 4a) follow that of steady-state QYs. For CdSe/CdS NRs, $MV^{+\bullet}$ radicals show negligible recombination within 10 μs, resulting in the near unity steady-state QY. Charge recombination is suppressed in this system because hole transfer from CdSe/CdS NRs to MPA (0.31 ns, measured by time-resolved PL decay) is much faster than the recombination of $MV^{+\bullet}$ radical with holes in CdSe/CdS NRs (320 ns, measured with TA). On the other hand, for core only QDs, hole removal by MPA and recombination with $MV^{+\bullet}$ radicals are similarly fast, leading to large recombination loss and small steady-state QY.[37]

We further investigated how the electronic structure of CdSe/CdS NRs can simultaneously facilitate fast electron transfer to MV^{2+}, slow down electron−hole recombination, and enable fast hole removal. Using type II ZnSe/CdS dot-in-rod

DOI: 10.1021/ar500398g
Acc. Chem. Res. 2015, 48, 851−859

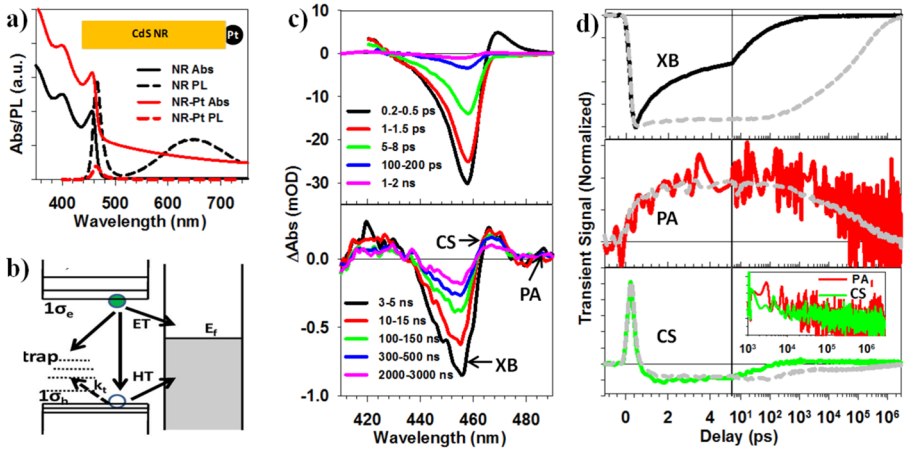

Figure 5. Exciton quenching mechanism in CdS−Pt NRs. (a) Absorption (solid lines, left axis) and emission (dashed lines, right axis) spectra of CdS NRs (black) and CdS−Pt NR heterostructures (red). (b) Schematic energy level and exciton quenching pathways in CdS−Pt NR heterostructures. (c) TA spectra of CdS−Pt NRs at indicated time delays: 0.2 ps to 2 ns (upper panel) and 3−3000 ns (lower panel). (d) TA kinetics of exciton bleach (XB, black solid line, top), photoinduced absorption (PA, red solid line, middle), and charge-separated state (CS, green solid line, bottom) spectral features for CdS−Pt NRs. Also shown for comparison are kinetics for free CdS NRs (gray dashed lines) at the same wavelengths. Inset: comparison of CS and PA kinetics in CdS−Pt after 1 ns. Adapted with permission from ref 18. Copyright 2012 American Chemical Society.

NRs as a model system,[43] we showed that the $MV^{+\bullet}$ radical generation QY of ZnSe/CdS NRs was ∼90% under 415 nm excitation, while the QY was much smaller (∼34%) under 550 nm excitation (Figure 4c). As shown in Figure 4d, in the presence of MV^{2+}, the charge transfer excitons created by 550 nm excitation are dissociated to form charge-separated state A with the hole in the ZnSe seed and electron in $MV^{+\bullet}$ radical adsorbed on the bulb region. The spatial proximity of the electron and hole leads to fast recombination, accounting for the lower steady-state QY (∼34%) of MV^{2+} photoreduction. Excitation into the CdS rod results in three types of charge-separated states: ∼70% are dissociated by ultrafast electron transfer to MV^{2+}, followed by hole localization into the core to generate charge-separated state C. Due to the long-distance separation of the electron and hole, charge recombination is effectively suppressed, leading to near unity steady-state QY of MV^{2+} photoreduction. The remaining pathways generate charge-separated states with both electrons and holes in the bulb/seed region (A, 13%) or in the rod region (B, 17%). The smaller electron−hole spatial separations in these pathways (A, B) lead to larger recombination loss and lower steady-state QYs. The ability to form long-distance charge-separated state C is the key for the high photoreduction efficiency of dot-in-rod structures, although this requires a fast electron receptor to compete with fast exciton localization to the seed.

6. CHARGE SEPARATION IN CdS−Pt AND CdSe/CdS−Pt HETERO-NANORODS

Selective deposition of metallic domains on the tips of NRs forms barbell or matchstick like metal−semiconductor heterostructures, such as the Pt tipped CdS (CdS−Pt) and CdSe/CdS (CdSe/CdS−Pt) NRs.[16,17,46−49] CdSe/CdS−Pt NRs are especially interesting because they can possibly transfer electrons into the Pt tip and localize holes in the CdSe core to form long-distance charge-separated states for efficient H_2 generation.[21]

We first examined the exciton quenching mechanism in CdS−Pt NRs. The absorption spectrum of CdS−Pt NRs (Figure 5a) shows broad features extending from UV to near IR, due to strong d−sp interband transition of platinum nanoparticles,[50] in addition to the excitonic peaks of CdS NRs. The PL spectrum of CdS−Pt NRs shows that both the CdS band edge and trap state emissions are strongly quenched by the Pt tip.[33] As shown in Figure 5b, excitons generated in the semiconductor NR can be quenched via electron, hole, and energy transfer to the metallic domain. The generation of H_2 requires the selective transfer of electrons from the semiconductor to the metal while suppressing other pathways.

We applied TA spectroscopy to investigate the competition between electron, hole, and energy transfer processes.[18] The TA spectra of CdS−Pt NRs at indicated delays after 400 nm excitation are shown in Figure 5c. Compared with free CdS NRs (Figure 5d), the exciton bleach (XB) in CdS−Pt NRs shows ultrafast decay, indicating depopulation of CB electrons in CdS NRs, while the PA signal (i.e., the trapped holes) remains unaffected. Since both hole and energy transfer processes reduce the hole signal, the observed ultrafast exciton quenching (∼3.4 ps) is solely due to electron transfer from the CdS NR to the Pt tip. The charge separation yield in this system is near unity because this quenching time is much shorter than electron lifetime in free NRs (∼100 ns).

Figure 5c (lower panel) also shows that XB recovery is accompanied by the formation of a derivative-like feature of exciton bands similar to that observed in CdS NR−electron acceptor complexes, which can be attributed to the $CdS^{+}-Pt^{-}$ charge-separated state (CS).[18] As shown in Figure 5d (middle and lower panels), CS and PA have a half-life of 1.2 ± 0.6 μs, indicating a long-lived charge-separated state. The large difference in charge separation and recombination rates can be rationalized by hole trapping on CdS NRs. Electrons can be dissociated from the trapped holes and diffuse rapidly through the rod to reach the Pt tip, leading to a fast electron transfer process, whereas holes are localized at the trap sites, slowing down the recombination process. This large difference in charge separation and recombination rates enables the removal of trapped holes in the presence of hole acceptors, leading to the accumulation of electrons in the Pt tip and photocatalytic H_2 production.[21,51]

The above result suggests that in these semiconductor−metal hetero-NRs, the immobilization of photogenerated holes is

DOI: 10.1021/ar500398g
Acc. Chem. Res. 2015, 48, 851−859

essential for efficient charge separation and long-lived charge-separated states. For this reason, CdSe/CdS−Pt dot-in-rod NRs should be a better system for this application because the hole can be localized to the VB of the CdSe core with known and controllable location and depth. However, due to the presence of three types of exciton species in CdSe/CdS NRs under rod excitation, the quenching processes of these excitons by the Pt tip needs to be examined separately.[22] Since X1 and X2 are associated with trapped holes on CdS NRs, their quenching should proceed through electron transfer to the Pt tip, similar to CdS−Pt. For X3 excitons, we estimated a slow energy transfer time constant of ∼38 ns, due to the long spatial separation between the CdSe core and the tip, which is too slow to be an efficient exciton quenching channel.[22]

The TA spectra of 400 nm excited CdSe/CdS−Pt at indicated delays are shown in Figure 6a. The B1, B2, and B3

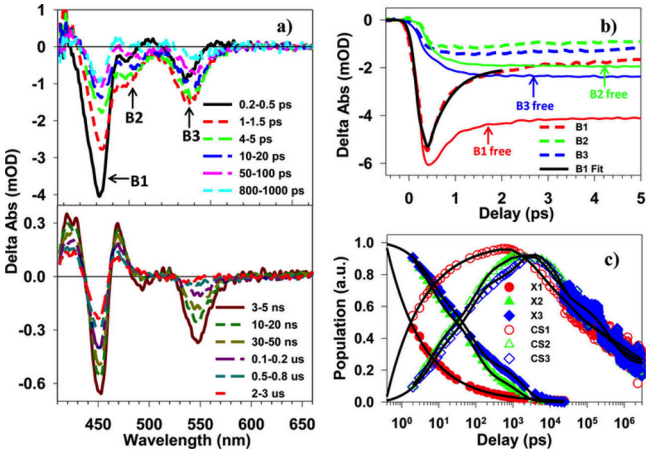

Figure 6. Transient absorption spectra and kinetics of CdSe/CdS−Pt measured with 400 nm excitation. (a) TA spectra of CdSe/CdS−Pt at indicated delay times from 0.2 ps to 3000 ns. (b) Kinetics of B1 (∼450 nm, red lines), B2 (∼480 nm, green line), and B3 (∼540 nm, blue line) of CdSe/CdS−Pt (dashed lines) and CdSe/CdS (solid lines) within 5 ps. The black solid line is a fit to B1 kinetics within 2 ps. (c) Time-dependent populations for X1 (red filled circles), X2 (green filled triangles), and X3 (blue filled diamonds) excitons and their charge-separated states CS1 (red open circles), CS2 (green open triangles), and CS3 (blue open diamonds) from 0.4 ps to 3000 ns. The black solid lines are multiexponential fits to these kinetics. Adapted with permission from ref 22. Copyright 2014 American Chemical Society.

bleaches recovered quickly with concomitant formation of derivative-like charge-separated state (CS) signals, similar to the formation of the CS signal in CdS−Pt NRs. The initial signal amplitudes of B2 and B3 were only 67% of those in free DIRs (Figure 6b), suggesting ultrafast electron transfer to Pt prior to the formation of X2 and X3. This is similar to the charge-separated state C observed in ZnSe/CdS NR−MV^{2+} complexes in Figure 4d. The time constant of this fast electron transfer process was τ_{fET} = 0.47 ps. The time-dependent populations for X1, X2, X3, CS1, CS2, and CS3 signals, obtained from fitting the TA spectra, are displayed in Figure 6c.[22] From these kinetics, we obtained half-lives of 1.75 ± 0.22, 30.1 ± 3.5, and 43.5 ± 4.7 ps for charge separation and 102 ± 29, 211 ± 38, and 211 ± 38 ns for charge recombination for X1, X2, and X3 excitons, respectively. It is interesting to note that our directly measured charge recombination time scales are similar to the value (∼100 ns) inferred from a single nanoparticle photoluminescence study on CdSe/CdS−Pt NRs.[52] Compared with free exciton lifetimes (Figure 4), the transient charge separation yields for three excitons all approach unity, and the charge-separated states are long-lived. In similar type II ZnSe/CdS−Pt NRs, ultrafast charge separation (with a time constant of 15 ps) has also been reported.[53] It is worth mentioning that all these ultrafast measurements to date only probed the first electron transfer event.[18,20,22,53] Considering that the H_2 generation reaction is a two-electron process, it is necessary in the future to design ultrafast spectroscopy experiments to measure charge separation and recombination rates for both electron transfer events.[53] This can also help answer a particular interesting question concerning the effect of Coulomb repulsion of the first electron on the second electron transfer step.[52,53]

7. CdS−Pt AND CdSe/CdS−Pt NANORODS FOR LIGHT-DRIVEN H_2 GENERATION

Despite near unity charge separation yields and long-lived charge-separated states of CdS−Pt and CdSe/CdS−Pt NRs, the best reported H_2 generation QY using these heterostructures is ∼20%.[21] To uncover the efficiency limiting steps, we correlated the observed H_2 generation efficiency with the rates of various processes shown in Scheme 1.[22] For this study, the NRs and NR−Pt heterostructures were transferred to aqueous phase using 11-mercaptoundecanoic acid (MUA) as ligands. MUA can act as sacrificial electron donors, but additional donors were added to maintain the dispensability of NRs. As shown in Figure 7, the steady-state H_2 generation

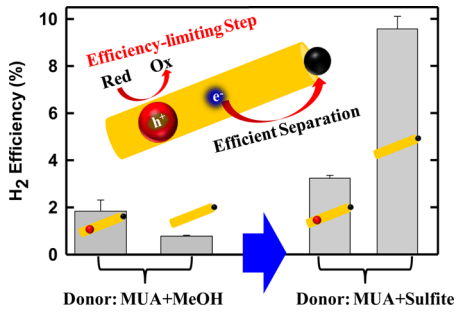

Figure 7. Steady state photodriven H_2 generation QYs using MUA-capped CdSe/CdS−Pt and CdS−Pt NRs, with either methanol or sodium sulfite as additional sacrificial electron donors. Adapted with permission from ref 22. Copyright 2014 American Chemical Society.

QYs using these nanorods depend on electron donors. With methanol as an electron donor, a higher QY is observed for CdSe/CdS−Pt (∼1.8%) than CdS−Pt (∼0.78%). With sulfite as an electron donor, the QY is improved for both, but the QY for CdS−Pt (∼9.6%) becomes higher than that for CdSe/CdS−Pt (∼3.2%).

The difference between the NR PL decay kinetics with and without sacrificial electron donors can be used to determine the hole transfer rates, which are summarized in Table 1. Clearly, there is a positive correlation between the hole transfer rates and H_2 generation QYs. Specifically, (i) the H_2 generation QYs and hole transfer rates are higher with sulfite than methanol for both CdS−Pt and CdSe/CdS−Pt NRs, and (ii) the relative QY follows the trend of hole transfer rates when CdS−Pt is compared with CdSe/CdS−Pt NRs. This positive correlation, combined with near unity initial charge separation yields, indicates that hole removal is an efficiency-limiting step in photocatalytic H_2 generation using these NR heterostructures.

DOI: 10.1021/ar500398g
Acc. Chem. Res. 2015, 48, 851−859

Table 1. Measured Apparent Hole Transfer Times and H_2 Generation Quantum QYs in CdS−Pt and CdSe/CdS−Pt NRs[22]

	CdS−Pt + MeOH		CdS−Pt + sulfite		CdSe/CdS−Pt + MeOH		CdSe/CdS−Pt + sulfite	
	MUA	MeOH	MUA	sulfite	MUA	MeOH	MUA	sulfite
apparent HT (ns)	0.218 ± 0.003	≫100	0.218 ± 0.003	0.0607 ± 0.018	0.0441 ± 0.008	≫100	0.0441 ± 0.008	0.154 ± 0.022
QE (H_2), %	0.78 ± 0.03		9.6 ± 0.5		1.8 ± 0.4		3.2 ± 0.1	

The hole removal rates of CdS and CdSe/CdS NRs by electron donors (<1 ns) are considerably faster than the rates of recombination between holes in NRs and electrons in Pt (≫1 ns). This result suggests that the holes that are transferred to MUA or to sulfite (i.e., the one-electron oxidized sulfite and MUA intermediate) may still recombine with electrons in Pt, reducing the H_2 generation efficiency. Therefore, efforts should be made to design electron donors that undergo ultrafast irreversible changes to close all the recombination channels for electrons in Pt.

8. SUMMARY AND OUTLOOK

In this Account, we summarize our recent studies of exciton dynamics in CdS NRs, CdSe/CdS NRs, NR−MV^{2+} complexes, and NR−Pt heterostructures. The key findings are the following. In CdS NRs, ultrafast hole trapping leads to long-lived trapped excitons (with CB electrons bound to the trapped holes). In CdSe/CdS dot-in-rod NRs, the competition between hole localization to the CdSe core and trapping on CdS rod leads to the formation of excitons localized in CdS rod, CdS bulb, and CdSe core. The branching ratio of these excitons depends on the excitation wavelength, which gives rise to excitation wavelength dependent steady-state quantum yields of MV^{2+} photoreduction in the presence of sacrificial electron donors. Compared with spherical quantum dots (core only or core/shell), CdSe/CdS NRs can achieve much higher (near unity) quantum yields of MV^{2+} photoreduction, which can be attributed to the ability to form long distance change separation along the axial direction in NRs. In NR−Pt, the localized excitons in CdS and CdSe/CdS NRs can dissociate efficiently by electron transfer to the Pt tip to form long-lived charge-separated states. In the presence of sacrificial electron donors, efficient light-driven H_2 evolution can be achieved, and its efficiency is limited by hole removal rates from these heterostructures.

Many issues remain to be investigated in future studies. In NR−Pt heterostructures, the excitons can be localized tens of nanometers away from the Pt tip but can still be efficiently dissociated by electron transfer to Pt. It is possible that charge separation proceeds by the dissociation of bound excitons to generate free CB electrons, which can then diffuse rapidly to reach the Pt tip, although concrete experimental evidence to support this model is lacking. Understanding the mechanisms for such long distance charge separation and recombination is essential to the rational optimization of these materials. Although hole removal is the key efficiency-limiting factor in light-driven H_2 generation in NR−Pt heterostructures, efficient hole removal schemes are still lacking. Furthermore, since the energetics of photogenerated holes in these quantum confined nanorods can in principle be tuned through size and composition, they should provide opportunities for photo-driven oxidation reactions.[54]

AUTHOR INFORMATION

Corresponding Author

*E-mail: tlian@emory.edu.

Funding

The authors gratefully acknowledge the financial support from the Office of Basic Energy Sciences of the U.S. Department of Energy (Grant No. DE-FG02-12ER16347).

Notes

The authors declare no competing financial interest.

Biographies

Kaifeng Wu received his B.S. degree in materials physics from the University of Science and Technology of China in 2010 and is a Ph.D. student at Emory University with Prof. Tianquan Lian. His research is focused on ultrafast charge carrier dynamics in photocatalytic semiconductor and semiconductor/metal hetero-nanostructures.

Haiming Zhu received his B.S. degree in Chemistry from the University of Science and Technology of China in 2008 and Ph.D. degree in Chemistry from Emory University in 2014. He is currently a postdoctoral fellow at Columbia University. His research focuses on carrier dynamics and charge transfer properties of quantum confined semiconductor nanomaterials and their applications in solar energy conversion.

Tianquan (Tim) Lian received his B.S. degree from Xiamen University in 1985, M.S. degree from the Chinese Academy of Sciences in 1988, and Ph.D. from the University of Pennsylvania in 1993. He is currently the William Henry Emerson Professor in the Department of Chemistry, Emory University. Tim Lian's research interests are focused on ultrafast dynamics in photovoltaic and photocatalytic nanomaterials.

REFERENCES

(1) Peng, X. G.; Manna, L.; Yang, W. D.; Wickham, J.; Scher, E.; Kadavanich, A.; Alivisatos, A. P. Shape Control of CdSe Nanocrystals. *Nature* **2000**, *404*, 59−61.

(2) Milliron, D. J.; Hughes, S. M.; Cui, Y.; Manna, L.; Li, J.; Wang, L.-W.; Alivisatos, A. P. Colloidal Nanocrystal Heterostructures with Linear and Branched Topology. *Nature* **2004**, *430*, 190−195.

(3) Li, H.; Kanaras, A. G.; Manna, L. Colloidal Branched Semiconductor Nanocrystals: State of the Art and Perspectives. *Acc. Chem. Res.* **2013**, *46*, 1387−1396.

(4) Shieh, F.; Saunders, A. E.; Korgel, B. A. General Shape Control of Colloidal CdS, CdSe, CdTe Quantum Rods and Quantum Rod Heterostructures. *J. Phys. Chem. B* **2005**, *109*, 8538−8542.

(5) Steigerwald, M. L.; Brus, L. E. Semiconductor Crystallites: A Class of Large Molecules. *Acc. Chem. Res.* **1990**, *23*, 183−188.

(6) Katz, D.; Wizansky, T.; Millo, O.; Rothenberg, E.; Mokari, T.; Banin, U. Size-Dependent Tunneling and Optical Spectroscopy of CdSe Quantum Rods. *Phys. Rev. Lett.* **2002**, *89*, No. 086801.

(7) Li, L.-s.; Hu, J.; Yang, W.; Alivisatos, A. P. Band Gap Variation of Size- and Shape-Controlled Colloidal CdSe Quantum Rods. *Nano Lett.* **2001**, *1*, 349−351.

(8) Shabaev, A.; Efros, A. L. 1D Exciton Spectroscopy of Semiconductor Nanorods. *Nano Lett.* **2004**, *4*, 1821−1825.

DOI: 10.1021/ar500398g
Acc. Chem. Res. 2015, 48, 851−859

(9) Zhu, H.; Lian, T. Wavefunction Engineering in Quantum Confined Semiconductor Nanoheterostructures for Efficient Charge Separation and Solar Energy Conversion. *Energy Environ. Sci.* **2012**, *5*, 9406−9418.
(10) Sitt, A.; Hadar, I.; Banin, U. Band-Gap Engineering, Optoelectronic Properties and Applications of Colloidal Heterostructured Semiconductor Nanorods. *Nano Today* **2013**, *8*, 494−513.
(11) Talapin, D. V.; Nelson, J. H.; Shevchenko, E. V.; Aloni, S.; Sadtler, B.; Alivisatos, A. P. Seeded Growth of Highly Luminescent CdSe/CdS Nanoheterostructures with Rod and Tetrapod Morphologies. *Nano Lett.* **2007**, *7*, 2951−2959.
(12) Carbone, L.; Nobile, C.; De Giorgi, M.; Sala, F. D.; Morello, G.; Pompa, P.; Hytch, M.; Snoeck, E.; Fiore, A.; Franchini, I. R.; Nadasan, M.; Silvestre, A. F.; Chiodo, L.; Kudera, S.; Cingolani, R.; Krahne, R.; Manna, L. Synthesis and Micrometer-Scale Assembly of Colloidal CdSe/CdS Nanorods Prepared by a Seeded Growth Approach. *Nano Lett.* **2007**, *7*, 2942−2950.
(13) Talapin, D. V.; Koeppe, R.; Götzinger, S.; Kornowski, A.; Lupton, J. M.; Rogach, A. L.; Benson, O.; Feldmann, J.; Weller, H. Highly Emissive Colloidal CdSe/CdS Heterostructures of Mixed Dimensionality. *Nano Lett.* **2003**, *3*, 1677−1681.
(14) Halpert, J. E.; Porter, V. J.; Zimmer, J. P.; Bawendi, M. G. Synthesis of CdSe/CdTe Nanobarbells. *J. Am. Chem. Soc.* **2006**, *128*, 12590−12591.
(15) Kirsanova, M.; Nemchinov, A.; Hewa-Kasakarage, N. N.; Schmall, N.; Zamkov, M. Synthesis of ZnSe/CdS/ZnSe Nanobarbells Showing Photoinduced Charge Separation. *Chem. Mater.* **2009**, *21*, 4305−4309.
(16) Mokari, T.; Rothenberg, E.; Popov, I.; Costi, R.; Banin, U. Selective Growth of Metal Tips onto Semiconductor Quantum Rods and Tetrapods. *Science* **2004**, *304*, 1787−1790.
(17) Habas, S. E.; Yang, P.; Mokari, T. Selective Growth of Metal and Binary Metal Tips on CdS Nanorods. *J. Am. Chem. Soc.* **2008**, *130*, 3294−3295.
(18) Wu, K.; Zhu, H.; Liu, Z.; Rodríguez-Córdoba, W.; Lian, T. Ultrafast Charge Separation and Long-Lived Charge Separated State in Photocatalytic CdS−Pt Nanorod Heterostructures. *J. Am. Chem. Soc.* **2012**, *134*, 10337−10340.
(19) Acharya, K. P.; Khnayzer, R. S.; O'Connor, T.; Diederich, G.; Kirsanova, M.; Klinkova, A.; Roth, D.; Kinder, E.; Imboden, M.; Zamkov, M. The Role of Hole Localization in Sacrificial Hydrogen Production by Semiconductor−Metal Heterostructured Nanocrystals. *Nano Lett.* **2011**, *11*, 2919−2926.
(20) Berr, M. J.; Vaneski, A.; Mauser, C.; Fischbach, S.; Susha, A. S.; Rogach, A. L.; Jäckel, F.; Feldmann, J. Delayed Photoelectron Transfer in Pt-Decorated CdS Nanorods under Hydrogen Generation Conditions. *Small* **2012**, *8*, 291−297.
(21) Amirav, L.; Alivisatos, A. P. Photocatalytic Hydrogen Production with Tunable Nanorod Heterostructures. *J. Phys. Chem. Lett.* **2010**, *1*, 1051−1054.
(22) Wu, K.; Chen, Z.; Lv, H.; Zhu, H.; Hill, C. L.; Lian, T. Hole Removal Rate Limits Photo-driven H_2 Generation Efficiency in CdS−Pt and CdSe/CdS−Pt Semiconductor Nanorod−Metal Tip Heterostructures. *J. Am. Chem. Soc.* **2014**, *136*, 7708−7716.
(23) Borys, N. J.; Walter, M. J.; Huang, J.; Talapin, D. V.; Lupton, J. M. The Role of Particle Morphology in Interfacial Energy Transfer in CdSe/CdS Heterostructure Nanocrystals. *Science* **2010**, *330*, 1371−1374.
(24) Wu, K.; Rodríguez-Córdoba, W. E.; Liu, Z.; Zhu, H.; Lian, T. Beyond Band Alignment: Hole Localization Driven Formation of Three Spatially Separated Long-Lived Exciton States in CdSe/CdS Nanorods. *ACS Nano* **2013**, *7*, 7173−7185.
(25) Mauser, C.; Da Como, E.; Baldauf, J.; Rogach, A. L.; Huang, J.; Talapin, D. V.; Feldmann, J. Spatio-temporal Dynamics of Coupled Electrons and Holes in Nanosize CdSe-CdS Semiconductor Tetrapods. *Phys. Rev. B* **2010**, *82*, No. 081306.
(26) Wu, K.; Rodríguez-Córdoba, W.; Lian, T. Exciton Localization and Dissociation Dynamics in CdS and CdS−Pt Quantum Confined Nanorods: Effect of Nonuniform Rod Diameters. *J. Phys. Chem. B* **2014**, *118*, 14062−14069.
(27) Puthussery, J.; Lan, A.; Kosel, T. H.; Kuno, M. Band-Filling of Solution-Synthesized CdS Nanowires. *ACS Nano* **2008**, *2*, 357−367.
(28) Hoang, T. B.; Titova, L. V.; Jackson, H. E.; Smith, L. M.; Yarrison-Rice, J. M.; Lensch, J. L.; Lauhon, L. J. Temperature Dependent Photoluminescence of Single CdS Nanowires. *Appl. Phys. Lett.* **2006**, *89*, No. 123123.
(29) Bartnik, A. C.; Efros, A. L.; Koh, W. K.; Murray, C. B.; Wise, F. W. Electronic States and Optical Properties of PbSe Nanorods and Nanowires. *Phys. Rev. B* **2010**, *82*, No. 195313.
(30) Vietmeyer, F.; McDonald, M. P.; Kuno, M. Single Nanowire Microscopy and Spectroscopy. *J. Phys. Chem. C* **2012**, *116*, 12379−12396.
(31) Brus, L. Size, Dimensionality, and Strong Electron Correlation in Nanoscience. *Acc. Chem. Res.* **2014**, *47*, 2951−2959.
(32) Brus, L. Commentary: Carbon Nanotubes, CdSe Nanocrystals, and Electron−Electron Interaction. *Nano Lett.* **2010**, *10*, 363−365.
(33) Saunders, A. E.; Ghezelbash, A.; Sood, P.; Korgel, B. A. Synthesis of High Aspect Ratio Quantum-Size CdS Nanorods and Their Surface-Dependent Photoluminescence. *Langmuir* **2008**, *24*, 9043−9049.
(34) Lupo, M. G.; Della Sala, F.; Carbone, L.; Zavelani-Rossi, M.; Fiore, A.; Lüer, L.; Polli, D.; Cingolani, R.; Manna, L.; Lanzani, G. Ultrafast Electron−Hole Dynamics in Core/Shell CdSe/CdS Dot/Rod Nanocrystals. *Nano Lett.* **2008**, *8*, 4582−4587.
(35) Müller, J.; Lupton, J. M.; Lagoudakis, P. G.; Schindler, F.; Koeppe, R.; Rogach, A. L.; Feldmann, J.; Talapin, D. V.; Weller, H. Wave Function Engineering in Elongated Semiconductor Nanocrystals with Heterogeneous Carrier Confinement. *Nano Lett.* **2005**, *5*, 2044−2049.
(36) Khon, E.; Lambright, K.; Khnayzer, R. S.; Moroz, P.; Perera, D.; Butaeva, E.; Lambright, S.; Castellano, F. N.; Zamkov, M. Improving the Catalytic Activity of Semiconductor Nanocrystals through Selective Domain Etching. *Nano Lett.* **2013**, *13*, 2016−2023.
(37) Zhu, H.; Song, N.; Lv, H.; Hill, C. L.; Lian, T. Near Unity Quantum Yield of Light-Driven Redox Mediator Reduction and Efficient H_2 Generation Using Colloidal Nanorod Heterostructures. *J. Am. Chem. Soc.* **2012**, *134*, 11701−11708.
(38) Jiang, Z.-J.; Kelley, D. F. Hot and Relaxed Electron Transfer from the CdSe Core and Core/Shell Nanorods. *J. Phys. Chem. C* **2011**, *115*, 4594−4602.
(39) Wu, K.; Rodríguez-Córdoba, W. E.; Yang, Y.; Lian, T. Plasmon-Induced Hot Electron Transfer from the Au Tip to CdS Rod in CdS-Au Nanoheterostructures. *Nano Lett.* **2013**, *13*, 5255−5263.
(40) Zhu, H.; Lian, T. Enhanced Multiple Exciton Dissociation from CdSe Quantum Rods: The Effect of Nanocrystal Shape. *J. Am. Chem. Soc.* **2012**, *134*, 11289−11297.
(41) Zhu, H.; Song, N.; Rodríguez-Córdoba, W.; Lian, T. Wave Function Engineering for Efficient Extraction of up to Nineteen Electrons from One CdSe/CdS Quasi-Type II Quantum Dot. *J. Am. Chem. Soc.* **2012**, *134*, 4250−4257.
(42) Lupo, M. G.; Zavelani-Rossi, M.; Fiore, A.; Polli, D.; Carbone, L.; Cingolani, R.; Manna, L.; Lanzani, G. Evidence of Electron Wave Function Delocalization in CdSe/CdS Asymmetric Nanocrystals. *Superlattices Microstruct.* **2010**, *47*, 170−173.
(43) Zhu, H.; Chen, Z.; Wu, K.; Lian, T. Wavelength Dependent Efficient Photoreduction of Redox Mediators Using Type II ZnSe/CdS Nanorod Heterostructures. *Chem. Sci.* **2014**, *5*, 3905−3914.
(44) Du, P.; Schneider, J.; Jarosz, P.; Eisenberg, R. Photocatalytic Generation of Hydrogen from Water Using a Platinum(II) Terpyridyl Acetylide Chromophore. *J. Am. Chem. Soc.* **2006**, *128*, 7726−7727.
(45) Kiwi, J.; Gratzel, M. Hydrogen Evolution from Water Induced by Visible Light Mediated by Redox Catalysis. *Nature* **1979**, *281*, 657−658.
(46) Banin, U.; Ben-Shahar, Y.; Vinokurov, K. Hybrid Semiconductor−Metal Nanoparticles: From Architecture to Function. *Chem. Mater.* **2014**, *26*, 97−110.

DOI: 10.1021/ar500398g
Acc. Chem. Res. 2015, 48, 851−859

(47) Menagen, G.; Macdonald, J. E.; Shemesh, Y.; Popov, I.; Banin, U. Au Growth on Semiconductor Nanorods: Photoinduced versus Thermal Growth Mechanisms. *J. Am. Chem. Soc.* **2009**, *131*, 17406−17411.
(48) Maynadié, J.; Salant, A.; Falqui, A.; Respaud, M.; Shaviv, E.; Banin, U.; Soulantica, K.; Chaudret, B. Cobalt Growth on the Tips of CdSe Nanorods. *Angew. Chem.* **2009**, *121*, 1846−1849.
(49) Saunders, A. E.; Popov, I.; Banin, U. Synthesis of Hybrid CdS−Au Colloidal Nanostructures. *J. Phys. Chem. B* **2006**, *110*, 25421−25429.
(50) Johnson, R. C.; Li, J.; Hupp, J. T.; Schatz, G. C. Hyper-Rayleigh Scattering Studies of Silver, Copper, And Platinum Nanoparticle Suspensions. *Chem. Phys. Lett.* **2002**, *356*, 534−540.
(51) Berr, M.; Vaneski, A.; Susha, A. S.; Rodriguez-Fernandez, J.; Doblinger, M.; Jackel, F.; Rogach, A. L.; Feldmann, J. Colloidal CdS Nanorods Decorated with Subnanometer Sized Pt Clusters for Photocatalytic Hydrogen Generation. *Appl. Phys. Lett.* **2010**, *97*, 093108.
(52) Amirav, L.; Alivisatos, A. P. Luminescence Studies of Individual Quantum Dot Photocatalysts. *J. Am. Chem. Soc.* **2013**, *135*, 13049−13053.
(53) O'Connor, T.; Panov, M. S.; Mereshchenko, A.; Tarnovsky, A. N.; Lorek, R.; Perera, D.; Diederich, G.; Lambright, S.; Moroz, P.; Zamkov, M. The Effect of the Charge-Separating Interface on Exciton Dynamics in Photocatalytic Colloidal Heteronanocrystals. *ACS Nano* **2012**, *6*, 8156−8165.
(54) Pirnot, M. T.; Rankic, D. A.; Martin, D. B. C.; MacMillan, D. W. C. Photoredox Activation for the Direct β-Arylation of Ketones and Aldehydes. *Science* **2013**, *339*, 1593−1596.

DOI: 10.1021/ar500398g
Acc. Chem. Res. 2015, 48, 851−859